I&EC research
Industrial & Engineering Chemistry Research

ARTICLE

pubs.acs.org/IECR

Global Kinetics for Ammonia Formation and Oxidation Reactions in a Commercial Three-Way Catalyst

Karthik Ramanathan,*[,†] Chander Shekhar Sharma,[‡,∥] and Chang Hwan Kim[§]

[†]General Motors Global Research and Development Center, India Science Lab, Bangalore, Karnataka, 560066, India

[‡]General Motors Powertrain, Bangalore, Karnataka, 560066, India

[§]General Motors Global Research and Development Center, Chemical Sciences and Materials Systems Lab, Warren, Michigan 48090, United States

ABSTRACT: Lean-burn spark ignition direct injection (SIDI) engines offer significant potential for improving engine efficiency and reducing greenhouse gas emissions. However, NO_x reduction in lean-burn SIDI engines presents significant challenges. One of the exhaust architectures that is currently being investigated and developed for lean-gasoline applications is the passive ammonia-SCR (three-way catalyst−selective catalyst reduction) system. It involves the use of the closed-coupled three-way catalyst (TWC) to generate NH_3 (during fuel-rich conditions) for use by the downstream NH_3−SCR for NO_x reduction. However, the NH_3 formed in TWC has to be controlled so that there is enough NH_3 for NO_x reduction in SCR, and at the same time, there is no NH_3 slip in the tailpipe. A mathematical model for the TWC, which can predict the net NH_3 coming out of the TWC, will be very useful for control algorithm development and for understanding and optimizing the exhaust architecture. The focus of this work is on the kinetic modeling of NH_3 formation and oxidation reactions in a three way catalyst (TWC). Controlled steady-state and transient test cell experiments were performed at different air-to-fuel ratios and different engine conditions. This data was used to expand the existing TWC global reaction to include three additional global reactions that can account for NH_3 formation and oxidation. A part of the experimental data was used to estimate the kinetic parameters of the above reactions (using a one-dimensional mathematical model for the TWC) through optimization techniques. The estimated kinetic parameters are able to predict the rest of the steady-state and controlled transient experimental data reasonably well.

INTRODUCTION

Lean-burn spark ignition direct injection (SIDI) engines offer significant benefit in improving fuel economy and reducing greenhouse gas emissions.[1,2] However, NO_x reduction in lean-burn SIDI engines presents significant challenges. Active NO_x abatement systems include selective catalytic reduction for NO_x by unburnt hydrocarbons (HC) present in engine exhaust (HC-SCR) or externally injected ammonia (urea) in the engine exhaust (NH_3−SCR), and storing of NO_x in the catalyst during lean engine operation and reducing it during short duration rich excursions (LNT, that is, lean NO_x trap). Urea-based SCR systems require a secondary fluid tank with an injection system resulting in added cost and complexity. LNT catalysts suffer from higher platinum group metal (PGM) costs and also from sulfur poisoning. At General Motors (GM), one of the exhaust architectures that are currently being investigated and developed for lean-gasoline applications is the urea-less passive ammonia-SCR (three-way catalyst−selective catalytic reduction catalyst) system.[3,4] It involves the use of the closed-coupled three-way catalyst (TWC), which apart from oxidizing the carbon monoxides, unburnt and partially burnt hydrocarbons, is used to generate NH_3 periodically (during fuel-rich conditions)[5] for use by the downstream NH_3−SCR for NO_x reduction (SCR stores the produced NH_3 and during lean operations the NO_x emissions are converted to N_2 over the SCR catalyst by using the stored reductant, NH_3). The major feature that distinguishes this innovative concept from other lean NO_x control technologies such as LNT or urea-SCR systems is that there is no need for high Pt-loaded sulfur intolerant NO_x trap or an extra urea tank to refill. One of the key factors that enable this technology is the efficient ammonia formation on the TWC and for maximizing the effectiveness of the passive ammonia-SCR system, it is important to maximize the efficiency of ammonia generation on the TWC. Generating ammonia over the TWC consumes fuel (because of the rich operation) and affects the overall efficiency for other regulated emissions such as CO and HC. The NH_3 formed during the rich operation in TWC has to be carefully tuned so that there is enough NH_3 for NO_x reduction in SCR during the lean operation and at the same time there is no NH_3 slip in the tailpipe. Therefore, it requires a rational design of the close-coupled TWC catalyst. A mathematical model for the TWC[6−8] that can predict the net NH_3 coming out of the TWC will be very useful for control algorithm development and for understanding and optimizing its exhaust architecture. In this work, we expand the standard set of reactions in a TWC model[6,8] to include the formation and oxidation of NH_3 and estimate the kinetic parameters for these reactions from controlled engine dynamometer data using a one-dimensional mathematical model for TWC.[6−8]

EXPERIMENTAL DATA

Steady-state as well as transient experimental data on TWC performance were collected from a stratified-charged direct-injection

Received: August 11, 2011
Accepted: December 7, 2011
Revised: November 11, 2011
Published: January 10, 2012

dx.doi.org/10.1021/ie2017866 | *Ind. Eng. Chem. Res.* 2012, 51, 1198–1208

Scheme 1. Arrangement of Front (FR) and Rear (RR) Bricks and Sampling Points.

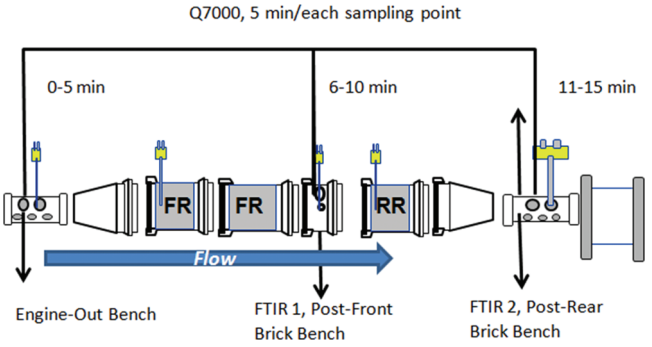

Table 1. Specification of the TWC Front Bricks

Ceria loading	0 g/ft^3
diameter (inches)	3.66
length (inches)	2.32
volume (liters)	0.40
cell density (cells per square inch)	600
washcoat thickness (milli- inches)	4.3
PGM loading, Pt/Pd/Rh ratio	200 g/ft^3, 0:1:0

engine in a transient engine dynamometer. The experiments were performed without the downstream SCR to understand the TWC performance. Arrangement of the various three way catalyst bricks and measurement points are shown in Scheme 1. The TWC used in these experiments had three bricks in series, two front bricks without any oxygen storage component such as Ceria and one rear brick with ceria and all of them were aged in the engine exhaust at around 1050 °C. Table 1 shows the TWC brick specifications for the front bricks. The engine was operated in both lean and rich operation modes by an in-house d-SPACE controller equipped with a Micro-Autobox. Steady-state data was obtained at three different engine conditions in terms of engine rpm and brake mean effective pressure: 1500 rpm and 1.5 bar (condition A), 2000 rpm and 2.0 bar (condition B) and 2800 rpm and 3.5 bar (condition C). For each condition, engine was run at various air to fuel ratio (AFR) conditions (14.8 to 14.0 in steps of 0.1). Under conditions A and C, the engine was run at each AFR for 900 s to reach steady-state. For condition B, engine was run at each AFR for 450 s to reach steady-state. Controlled transient data was also obtained under same conditions of engine rpm, exhaust pressure and similar AFR. For each AFR, the engine was run very lean (AFR = ~25) for 120 s followed by the specified AFR (14.6−13.8, in steps of 0.1) for 60 s.

To measure species concentrations for each AFR, HORIBA analyzers (bench) and MKS FTIR (Fourier Transform Infra-Red Spectroscopy) were used at engine-out, post-front brick and post-rear brick locations. [Note: Unless mentioned otherwise, we shall refer to "post-front brick" as the location after the two front bricks, that is, before the rear brick, please refer to Scheme 1]. Species concentrations for CO, HC, NO_x, and O_2 were measured in this manner. In addition to these species, H_2 concentrations were measured using Q7000 analyzer (Mass Spectrometer) by sampling sequentially at each of the three locations during the total run-time for each AFR. For example, in case of steady-state

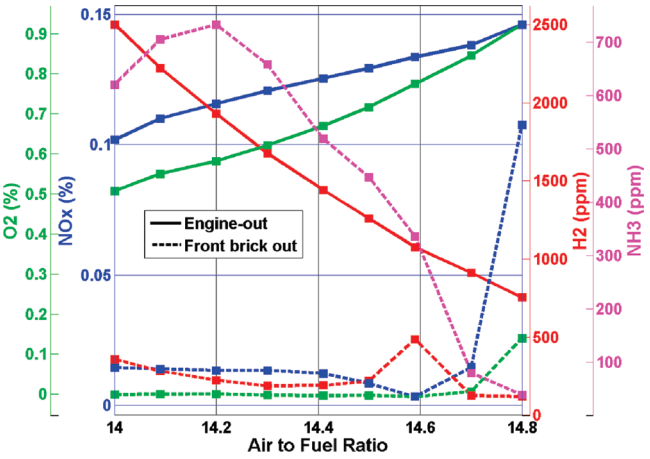

Figure 1. Engine-out and post-front brick molefractions of O_2, NO_x, NH_3, and H_2 for engine conditions of 1500 rpm and 1.5 bar (condition A).

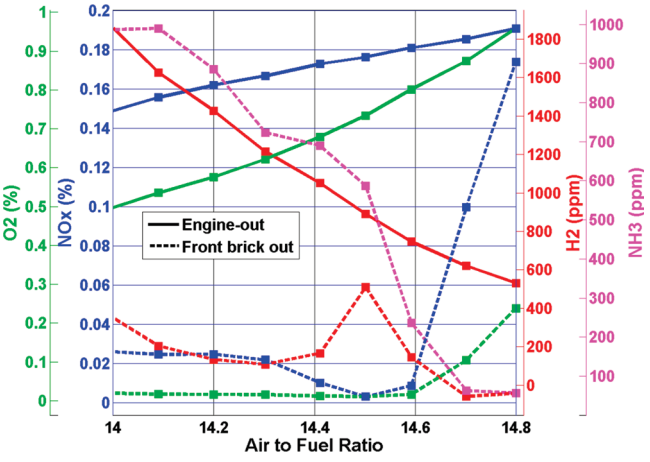

Figure 2. Engine-out and post-front brick molefractions of O_2, NO_x, NH_3, and H_2 for engine conditions of 2000 rpm and 2 bar (condition B).

data corresponding to 2800 rpm and 3.5 bar (i.e., condition C), H_2 concentrations were sampled for 300 s at each of the three locations of engine-out, post-front brick and post-rear brick. Steady-state data points were extracted from these measurements. However, for the case of controlled transient data H_2 measurements at post-front bricks location were not available.

PROCESSING OF EXPERIMENTAL DATA

Steady-State Data. As discussed in the previous section, steady-state data was obtained for 9 AFRs (14.8−14.0 in steps of 0.1) for each engine condition. For each AFR, steady-state values of measured flow rate, engine-out gas temperature, front brick 1 inch bed temperature and species concentrations (except for hydrogen) at engine-out, post-front brick and post-rear brick locations were obtained by linearly averaging the corresponding quantities over the time of run for each AFR. In case of hydrogen, as discussed in previous section, the measurements were made by sequentially placing Q7000 analyzer at each of the engine-out, post-front brick and post-rear brick locations for 300 s (in case of engine conditions A and C) or 150 s (in case of engine conditions B) during engine run for each AFR. At each

dx.doi.org/10.1021/ie2017866 |Ind. Eng. Chem. Res. 2012, 51, 1198–1208

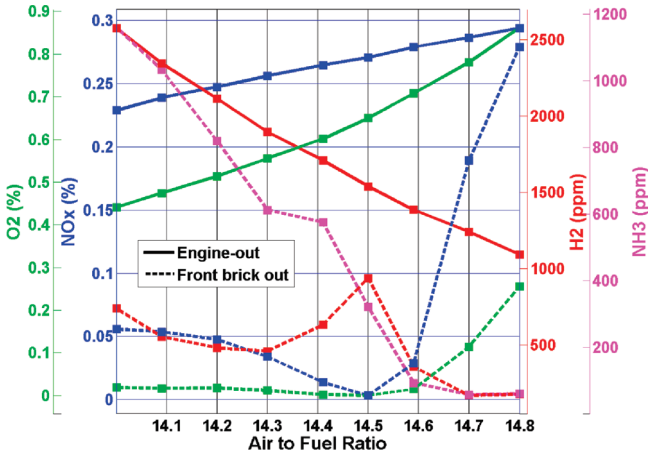

Figure 3. Engine-out and post-front brick molefractions of O_2, NO_x, NH_3, and H_2 for engine conditions of 2800 rpm and 3.5 bar (condition C).

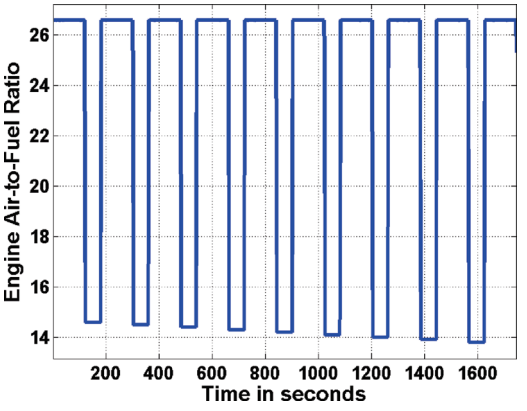

Figure 4. Engine air-to-fuel ratio variation with time for controlled transient experiments.

location (i.e., engine-out, post-front brick and post-rear brick), hydrogen concentration was not stable initially due to the slow response of the analyzer. Hence for each measurement location, hydrogen concentration was averaged over that part of the sampling time (corresponding to that location) where instantaneous H_2 concentration was stable. These experiments were repeated for three different engine conditions and hence there were a total of 27 steady-state data points. Figures 1, 2, and 3 show the steady-state mole-fractions of NH_3, O_2, H_2, and NO_x at engine-out and post-front brick location for three different engine conditions (A, B, C), respectively. It is observed that at lower engine load conditions (condition A), the NH_3 concentration at post-front brick outlet goes through a maximum (refer to Figure 1) as the AFR progresses from rich (14.0) to lean values (14.8). However, at higher engine load conditions, the NH_3 concentrations are monotonically decreasing as the AFR progresses from rich to lean values.

Controlled Transient Data. In case of this data, as mentioned before, for each AFR, the engine was run very lean for 120 s followed by the specified AFR for 60 s and this was performed for three different engine conditions (A, B, C). Figure 4 shows the time variation of the AFR variation for the entire operation and as can be seen the AFR changes from 14.6 to 13.8 in steps of 0.1 with lean operation in between them.

Table 2. Main Reactions in TWC

S. no.	reactions
	oxidation reactions
1	$CO + 0.5O_2 \rightarrow CO_2$
2	$C_3H_6 + 4.5O_2 \rightarrow 3CO_2 + 3H_2O$
3	$C_3H_8 + 5O_2 \rightarrow 3CO_2 + 4H_2O$
4	$H_2 + 0.5O_2 \rightarrow H_2O$
	NO reduction reactions
5	$CO + NO \rightarrow CO_2 + 0.5\ N_2$
6	$C_3H_6 + 9NO \rightarrow 3CO_2 + 3H_2O + 4.5N_2$
7	$H_2 + NO \rightarrow H_2O + 0.5N_2$
	water-gas and steam reforming reactions
8	$CO + H_2O \rightarrow CO_2 + H_2$
9	$C_3H_6 + 3H_2O \rightarrow 3CO + 6H_2$
	redox reactions over ceria
10	$2Ce_2O_3 + O_2 \rightarrow 4CeO_2$
11	$Ce_2O_3 + NO \rightarrow 2CeO_2 + 0.5N_2$
12	$CO + 2CeO_2 \rightarrow Ce_2O_3 + CO_2$
13	$C_3H_6 + 12CeO_2 \rightarrow 6Ce_2O_3 + 3CO + 3H_2O$
14	$C_3H_8 + 14CeO_2 \rightarrow 7Ce_2O_3 + 3CO + 4H_2O$
15	$H_2 + 2CeO_2 \rightarrow Ce_2O_3 + H_2O$

MODIFICATION IN TWC KINETICS MODEL

A single-channel (i.e., channel-to-channel variations and interactions are ignored) one-dimensional transient model is used for describing the monolith converter. The model equations, assumptions, and other correlations/details can be found in Ramanathan and Sharma.[8] The time-dependent terms are dropped when used for simulating steady-state experimental conditions. The global reaction mechanism incorporated in the existing TWC model[8] does not have NH_3 formation and oxidation reactions and has a total of 15 global reactions as listed in Table 2. The expansion of the global kinetic scheme for the three-way catalyst to account for NH_3 formation/oxidation reactions needs to be constructed with a minimum set of reactions (while capturing the necessary level of details to describe the experimentally observed phenomena) and its kinetic parameters need to be estimated from experimental data.

NH_3 is produced in the three-way catalyst under certain conditions[9] when NO is reduced by H_2. However, the formed NH_3 can get oxidized by the NO and the O_2 present in the reactor.[10−15] Additionally, it has been observed that any source of O-atoms in the system (not necessarily limited to O-atoms from NO or O_2) can oxidize the formed NH_3 to N_2 or N_2O.[11] It has been observed that at high temperatures, NH_3 oxidation reactions with NO and O_2 are active[10,16] and that NO reduction with NH_3 is as effective as NO reduction with H_2.[10,11] Note that NH_3 oxidation with NO_2 does not happen at these high temperatures as there were negligible amounts of NO_2 in the engine exhaust. In addition, on the TWC, the NO-NO_2 equilibrium favors NO at these temperatures. [Note: If NO_2 was present in the feed or is formed in the reactor, it is possible that some of the NH_3 gets oxidized with NO_2 and NO through a typical fast-SCR (Selective Catalytic Reduction) reaction or NH_3 gets oxidized with NO_2 to form N_2O[17]]. Among the NH_3 formation and oxidation reactions, it has been observed that the formation reaction is much faster than the oxidation with NO.[12] When NH_3 is oxidized with O_2, the possible products of oxidation are NO,

N_2O, or N_2 and when NH_3 is oxidized with NO, the possible products are N_2O and N_2. Most experiments[10−14] have shown that the N_2O formed is typically very less and occurs only at lower temperatures[15] and that NH_3 oxidation with NO yields N_2 as the primary product at higher temperatures.[15] We also find that there is very little N_2O formed in our experiments. However, there has not been any conclusive evidence of whether NH_3 oxidation with O_2 yields NO or N_2 and this behavior may be temperature dependent.[15] Some research articles assume that N_2 is the primary product of NH_3 oxidation with O_2.[10−12,14] TAP (Temporal Analysis of Products) reactor analysis shows that NO is a primary product of NH_3 oxidation with O-atoms and N_2 results mainly from secondary transformations of the formed NO.[13] Pihl et al.[15] observe that at low temperatures N_2 is the primary product of NH_3 oxidation with O_2 and at higher temperatures NO is the primary product of this reaction. For this work, we assume that NH_3 oxidation with O_2 gives NO as the primary product as our experiments predominantly see higher temperatures.

Though most of the reaction mechanism studies on NH_3 formation/oxidation on PGM catalyst have been studied on a Lean NO_x Trap (LNT) system, these can be applied to a Three-Way catalyst because the catalyst (PGM) compositions are similar. [Note: LNT has additional NO_x storage materials (like Barium) which help in storing NO_x because of which there would be additional reactions in a LNT]. There are detailed microkinetic models for predicting NH_3 oxidation reactions,[18,19] and there are also detailed microkinetic models for a LNT system which include NH_3 formation and oxidation.[14] A rate mapping approach that can predict ammonia oxidation reactions has also been presented.[20] However, our interest in this work is to have a global kinetic model for NH_3 formation/oxidation on a Three-Way Catalyst. There are global kinetic models for LNT which include NH_3 formation/oxidation reactions but the reaction parameters are not mentioned[16,21,22] and the actual kinetic parameters are likely to be different between a commercial LNT catalyst and a commercial TWC. On the basis of the above observations and discussions, three new reactions were added to the global reaction mechanism[6,8] to capture NH_3 formation and NH_3 oxidation with NO and O_2. These new reactions and the corresponding reaction rate expressions are described below:

(i) NH_3 oxidation with oxygen (reaction no. 16)

$$NH_3 + 1.25O_2 \rightarrow NO + 1.5H_2O$$

$$\text{Rate}(16) = \frac{k_{16} c_{NH_3} c_{O_2} \exp\left(-\frac{E_{16}}{R_g T_s}\right)}{G} = \frac{K_{16} c_{NH_3} c_{O_2}}{G}$$

(ii) NH_3 formation (reaction no. 17)

$$NO + 2.5H_2 \rightarrow NH_3 + H_2O$$

$$\text{Rate}(17) = \frac{k_{17} c_{H_2} c_{NO} \exp\left(-\frac{E_{17}}{R_g T_s}\right)}{G} = \frac{K_{17} c_{H_2} c_{NO}}{G}$$

(iii) NH_3 oxidation with NO (reaction no. 18)

$$NH_3 + 1.5NO \rightarrow 1.25N_2 + 1.5H_2O$$

$$\text{Rate}(18) = \frac{k_{18} c_{NH_3} c_{NO} \exp\left(-\frac{E_{18}}{R_g T_s}\right)}{G} = \frac{K_{18} c_{NH_3} c_{NO}}{G}$$

where G is the inhibition term (as given in ref 8). It should be mentioned that the same inhibition terms are used for the NH_3 formation and oxidation reactions as these reactions are assumed to occur on the same catalyst sites. In the above expressions, K_{16}, K_{17}, and K_{18} are the reaction rate constants for reactions 16, 17, and 18, respectively. The kinetic parameters for the other reactions are taken from Ramanathan and Sharma.[8] [Note: There is a possibility of the NH_3 formed to decompose to N_2 at higher temperatures.[15] However, it is expected that the reaction rates of NH_3 with NO or O_2 may be higher than NH_3 decomposition at the temperatures considered in this work and hence this reaction is not considered this work. Additionally, including all the possible reactions for NH_3 formation/consumption will increase the number of parameters to be estimated and since these parameters are being estimated for the first time, it is better to include the "most dominant reactions" that can capture the observed trends and then expand the reaction mechanism further].

The kinetic parameters for NH_3 formation and oxidation reactions are estimated through optimization techniques by minimizing the error between predicted and measured post-front brick NH_3.The details of the formulation of objective functions, data points included for the parameter estimation process and the optimization strategy are given in the Appendix.

PARAMETER ESTIMATION RUNS AND RESULTS

As mentioned earlier, a transient one-dimensional mathematical model for the three way catalyst[8] was used for simulation purposes. A steady-state version of the model (referred to as the "steady-state code" (SSC) hereon) is used to simulate the steady-state data points. Because of the nonlinear coupling involved in the system of equations, it is possible that the SSC is not able to solve the system of equations directly and in such cases, we use the transient model (simulated for sufficiently long time to reach steady-state) to obtain steady-state results. However, it is possible that the transient code can also fail because of (1) very stiff and unrealistic kinetic parameters or (2) steady-state multiplicities as a result of interactions between reaction kinetics and mass-transfer resistances.[23] Numerical issues arising because of the multiple solutions are explained in detail by Oh et al.[24] If both the steady-state and transient simulations failed for a particular combination of optimization parameters, then objective function was set to a very high value (10^{10}) as means of imposing high penalty for that combination of kinetic parameters. In addition to the above considerations, optimization runs were setup and performed for front bricks only. This was because the front bricks did not have ceria and this avoided the need to include any possible NH_3−ceria reactions/interactions which would increase the number of parameters to be estimated and increase the complexity of the parameter estimation process.

Although the optimization runs gradually evolved as the work progressed, overall, two parallel approaches were followed:

Approach (a). Minimize f given by eq A5 (in Appendix) and estimate reaction rate constants [$K_i = k_i \exp(-E_i/(R_g T_s))$] of reactions involving ammonia separately for each of the steady-state data-points. The pre-exponentials (k_i) and activation energies (E_i) of the reactions are then obtained by a linear fit of the $\log_e(K_i)$ versus $(1/T_{s,i})$ data points (Arrhenius plot).

dx.doi.org/10.1021/ie2017866 |Ind. Eng. Chem. Res. 2012, 51, 1198–1208

Approach (b). Minimize total objective function f_{total} (obtained by averaging f over all the *admissible* data-points as given in eq 1) to directly estimate pre-exponents (k_i) and activation energies (E_i) for ammonia reactions for all the *admissible* data-points (npt). (Please refer to Appendix for explanation on *admissible* data-points).

$$f_{total} = \frac{1}{npt}\sum_{i=1}^{npt} f \quad (1)$$

For estimating kinetic parameters using steady-state data, *approach (a) and approach (b)* were used. When using the steady-state data for calibration/estimation purposes, the controlled transient data was used for parameter validation purposes. For estimating kinetic parameters using controlled transient data, *approach (b)* was followed. When using the controlled transient data, engine condition A was used for parameter estimation purposes and engine conditions B, C and steady-state data were used for parameter validation purposes. Table 3 gives the details of the various data sets used for calibration and validation purposes along with information on the kinetics sets (which will be discussed later in this section).

Parameter estimation was first performed for the steady state data using *approach (a)* because initial estimates of the rate parameters for the NH_3 reaction kinetics were not available. *Approach (a)* gradually evolved as the optimization runs progressed. It was found that independently optimizing reaction rate constants for different steady-state data-points resulted in very poor fits in estimating pre-exponents and activation energies and hence, the below-mentioned methodology was followed:

(a) Additional rate-constant constraints were imposed on optimization runs for successive data-points as below: For ith reaction (i = 16, 17, 18) and for jth data-point (j = 1 to npt), if $T_{dmn} \le T_j \le T_{dmx}$, where T_j is the measured bed temperature for the jth data-point and dmn and dmx denote the data points with minimum and maximum measured bed temperature (among data-points 1 to $j-1$) respectively, then reaction rate constant $K_{i,j}$ is constrained as $K_{i,dmn} \le K_{i,j} \le K_{i,dmx}$. This was required in order to ensure that the estimated reaction rate constants for different data points would follow a monotonically increasing trend with increasing the temperature thus resulting in negative slope (Arrhenius-type) of linear fit for $\log_e(K_i)$ versus $(1/T_{s,i})$ data points.

(b) With the rate-constant constraint, the degree of success of optimization runs was influenced by the order in which the steady-state data-points were presented to the optimizer. It was observed that arranging the steady-state data-points in the descending order of post-front brick NH_3 concentration gave the best results.

However, despite such modifications, *approach (a)* could not successfully optimize reaction rate constants for all the admissible data-points. Because of the inability to estimate reaction rate constants for all the steady-state data-points, *approach (b)* was also tried. However, it was found that including all the data-points in optimization led to either unsuccessful completion of the optimization algorithm or very high final value for objective function. *Approach (b)* worked if only those data-points were included in optimization for which the optimizer had successfully optimized reaction rate constants in *approach (a)*.

Both the approaches were followed interchangeably and multiple sets of kinetics for NH_3 reactions were obtained. From among these sets, two sets of kinetics were shortlisted based on magnitude of pre-exponents (of the order of 10^{10} to 10^{20} were retained), quality of fits and magnitude of objective function. These are listed as "Kinetics Set 1" and "Kinetics Set 2" in Table 4. Apart from the reaction parameters listed in Table 4, kinetic parameters in the global reaction mechanism mentioned in Table 2 are obtained from Ramanathan and Sharma[8] and termed "A4 Kinetics". However, the pre-exponent for the reaction 5 in A4 kinetics[8] ($CO + NO \rightarrow CO_2 + 0.5N_2$) was reduced by an order of magnitude (to avoid NO being entirely consumed through this reaction) and was fixed at the reduced value throughout the optimization runs.

Activation energies in both the sets were similar except for NH_3 formation reaction. Pre-exponents in the sets were significantly different. Specifically, pre-exponent of NH_3 formation reaction was very high in case of Kinetics Set 1 because of the wide difference in activation energy among set 1 and set 2. Overall, performance for both the kinetics was similar for steady-state data. Figure 5 shows the predictions for post-front brick NH_3 mole-fraction using Kinetics Set 2. The x-axis labels represent

Table 3. Data Sets Used for Calibration/Validation Purposes for the Different Kinetics Sets

Kinetics Set no.	data used for calibration purposes	data used for validation/prediction purposes
1	all steady-state data points	controlled transient data—engine condition A
2	all steady-state data points	controlled transient data—engine condition A
3	controlled transient data—engine condition A	controlled transient data—engine condition B, C and all steady-state data-points

Table 4. Kinetic Parameters Estimated Using Steady-State Data

		Kinetics Set 1		Kinetics Set 2	
reaction no.	reaction	k	E	k	E
16	$NH_3 + 1.25\ O_2 = NO + 1.5\ H_2O$	$2.154 \times 10^{+10}$	$1.212 \times 10^{+5}$	$1.398 \times 10^{+12}$	$1.546 \times 10^{+5}$
17	$NO + 2.5\ H_2 = NH_3 + H_2O$	$1.000 \times 10^{+20}$	$1.414 \times 10^{+5}$	$7.890 \times 10^{+13}$	$4.698 \times 10^{+4}$
18	$NH_3 + 1.5\ NO = 1.25N_2 + 1.5\ H_2O$	$4.084 \times 10^{+15}$	$1.414 \times 10^{+5}$	$9.496 \times 10^{+16}$	$1.738 \times 10^{+5}$
5	$CO + NO = CO2 + 0.5\ N_2$	k fixed at $2.857 \times 10^{+8}$ (reduced by a factor of 10 from A4 kinetics), E kept fixed at A4 value			
others	same as A4 kinetics	k, E fixed at A4 values			

dx.doi.org/10.1021/ie2017866 |*Ind. Eng. Chem. Res.* 2012, 51, 1198–1208

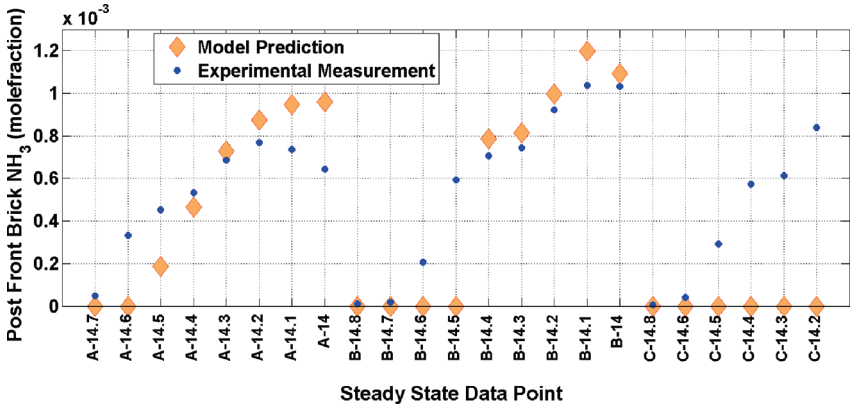

Figure 5. Predictions for post-front brick NH_3 using Kinetics Set 2. *X*-axis label represent the engine condition (A, B, C) and the air-to-fuel ratio. Engine condition A: 1500 rpm/1.5 bar; B: 2000 rpm/2 bar; C: 2800 rpm/3.5 bar.

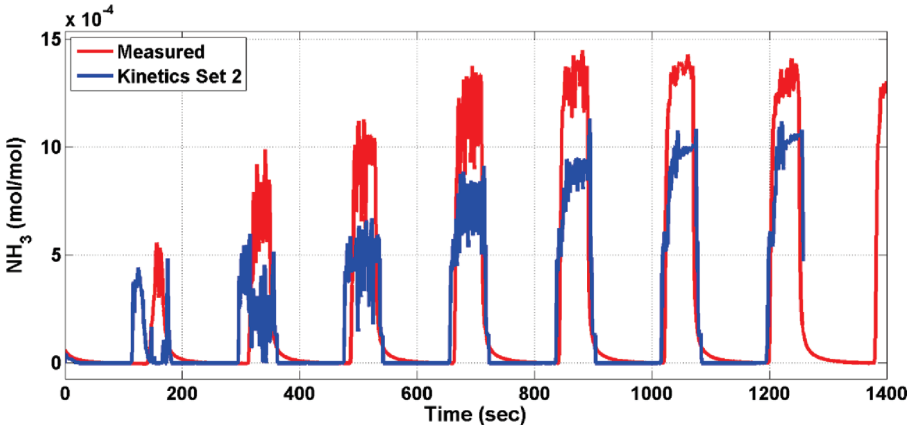

Figure 6. Performance of Kinetics Set 2 for controlled transient data 1500 rpm, 1.5 bar.

the engine condition (A, B, or C) and the air-to-fuel ratio. For example, C-14.5 represents condition-C with an air-to-fuel ratio of 14.5. As can be seen, these kinetics sets are not able to predict NH_3 formation in front brick for some of the steady-state data-points and even the qualitative trend of capturing the maximum in NH_3 concentration for engine condition A is not captured. The model predicts a monotonic behavior whereas the experiments show a maximum in NH_3 concentration for condition A.

Performance of these kinetics sets was validated to predict the controlled transient data. Figure 6 shows the performance of Kinetics Set 2 for controlled transient data corresponding to engine condition A. Performance of Kinetics Set 1 is similar to Set 2 and hence not shown in the figure. These kinetics sets are not able to simulate the transient data for full test time. A possible reason for the numerical difficulty could be that the kinetic parameters were obtained at high temperatures (>550 °C, using steady-state data) and hence may not be able to perform well at lower temperatures (which are observed for the controlled transient data). Figures 7 and 8 show the bed temperature (for various air-to-fuel ratios and engine conditions) for steady-state and controlled transient experiments, respectively. As can be observed, the temperatures in steady-state experiments are above 550 °C and the temperature in the controlled transient experiments varies from a low of 350 °C to a high of around 750 °C. The controlled transient data had wider temperature transients than the steady-state data and

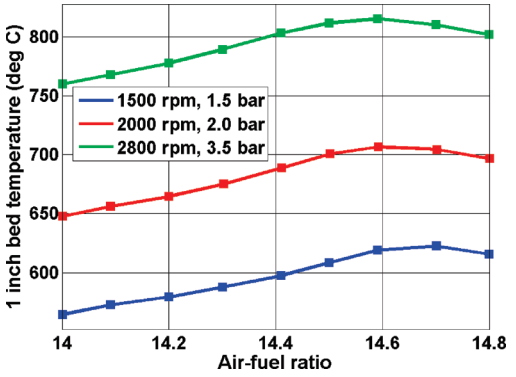

Figure 7. Steady-state data spread.

hence it is possible that the kinetics obtained using the steady-state data is not able to predict at lower temperatures.

As the kinetics estimated using the steady-state data did not perform well for the controlled transient data and since the control transient data is expected to contain more kinetic information (because of wider temperature window), a fresh set of kinetic parameters were estimated using the controlled transient data by following *approach (b)* using Kinetics Set 2 as a starting point. These new kinetic parameters, designated as Kinetics Set 3,

are shown in Table 5. While progressing through the optimization runs, we observed that peaks of NH_3 formation during controlled transients were not adequately captured by including only the kinetics parameters for NH_3 reactions among optimization parameters. In order to obtain Kinetics Set 3, pre-exponentials for a few other reactions involving NO and H_2 (reaction numbers 4, 5, 6, 7) had to be included in the list of optimization parameters as capturing kinetics of reactions involving NO and H_2 is critical for modeling NH_3 formation in TWC. Activation energies for these reactions were kept fixed at their respective A4 kinetics values. These reactions and the corresponding estimated pre-exponents are also listed in Table 5. The activation energies obtained in Table 5 are closer to those of the rate limiting steps mentioned by Xu et al.[25] and Vajo et al.[26] Preliminary sensitivity analysis shows that the pre-exponential factor of the NH_3 formation reaction (reaction number 17) is one of the highly sensitive parameters followed by the activation energy of the ammonia oxidation reaction with NO (reaction number 18) followed by the activation energy of the ammonia oxidation reaction with O_2 (reaction number 16). This sensitivity analysis was based on the ammonia predicted at the post-front brick location. The pre-exponential factors of the ammonia oxidation reactions with NO and O_2 are not very sensitive. However, the results of the sensitivity analysis are specific to experimental conditions and cannot be directly extended to the different experimental conditions. [Note: Since the kinetic parameters are obtained using data from high temperatures, it is found that very similar quantitative results can be obtained using an activation energy value between 44.72 and 54.72 kJ for the NH_3 formation reaction (with a corresponding change in the pre-exponential factor so that the rate constant at 600 $^{\circ}$ C is the same), and this uncertainty in the activation energy can be resolved only by fitting the parameters to low temperature data].

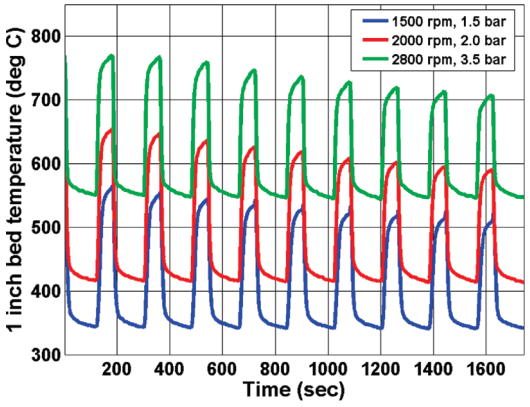

Figure 8. Controlled transient data spread.

Controlled transient data corresponding to engine condition A was used for parameter estimation (to obtain Kinetics Set 3) and conditions B and C were used for validation. As mentioned earlier, for the sake of completeness and easy understanding, the data sets used for calibration and validation for the different kinetic sets are given in Table 3. Figure 9 shows the calibration performance of Kinetics Set 3 for controlled transient data pertaining to engine condition A. The peaks of post-front brick NH_3 are captured reasonably well. However, there is a certain time lag between the predicted and measured NH_3 peaks.

Table 5. Kinetic Parameters Estimated Using Controlled Transient Data

		Kinetics Set 3	
reaction no.	reaction	*k*	*E*
16	$NH_3 + 1.25\ O_2 = NO + 1.5\ H_2O$	$1.000 \times 10^{+10}$	$1.693 \times 10^{+5}$
17	$NO + 2.5\ H_2 = NH_3 + H_2O$	$6.813 \times 10^{+10}$	$4.472 \times 10^{+4}$
18	$NH_3 + 1.5\ NO = 1.25N_2 + 1.5\ H_2O$	$1.000 \times 10^{+10}$	$1.214 \times 10^{+5}$
4	$H_2 + 0.5\ O_2 = H_2O$	$1.668 \times 10^{+13}$	*E* kept fixed at A4 values
5	$CO + NO = CO2 + 0.5\ N_2$	$2.154 \times 10^{+9}$	
6	$C_3H_6 + 9\ NO = 3\ CO_2 + 3\ H_2O + 4.5\ N_2$	$4.642 \times 10^{+9}$	
7	$NO + H_2 = 0.5\ N_2 + H_2O$	$4.642 \times 10^{+8}$	
others	same as A4 kinetics	*k*, and *E* fixed at A4 values	

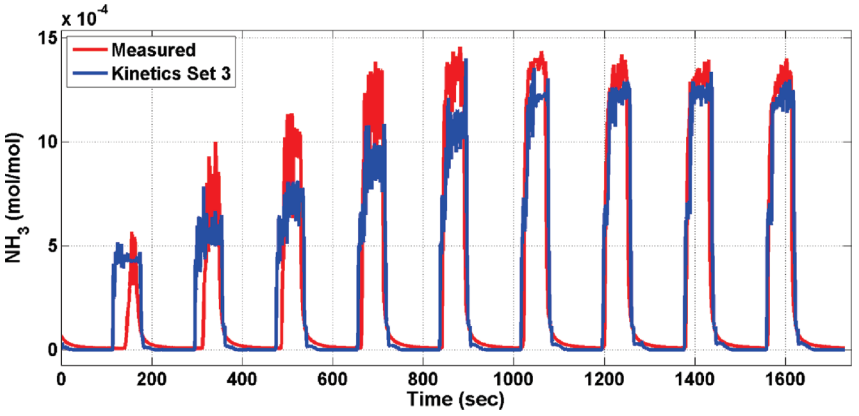

Figure 9. Performance of Kinetics Set 3 for controlled transient data 1500 rpm, 1.5 bar (engine condition A).

dx.doi.org/10.1021/ie2017866 |*Ind. Eng. Chem. Res.* 2012, 51, 1198–1208

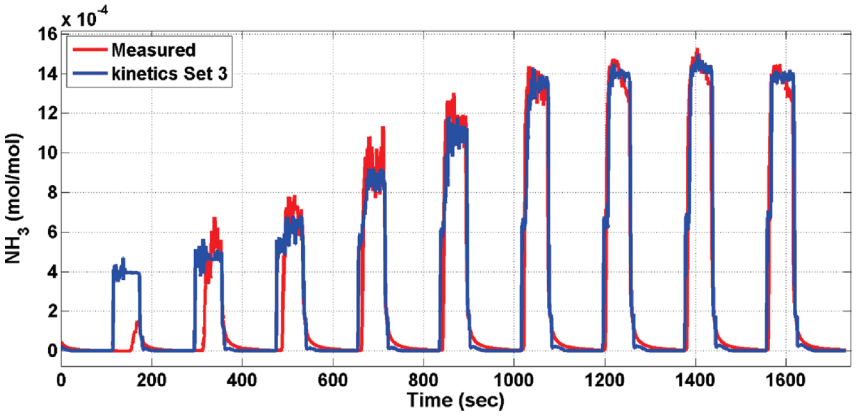

Figure 10. Performance of Kinetics Set 3 for controlled transient data 2000 rpm, 2.0 bar (engine condition B).

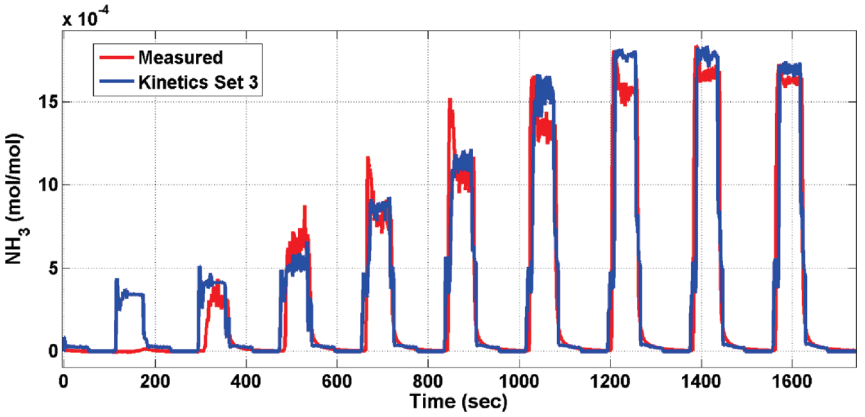

Figure 11. Performance of Kinetics Set 3 for controlled transient data 2800 rpm, 3.5 bar (engine condition C).

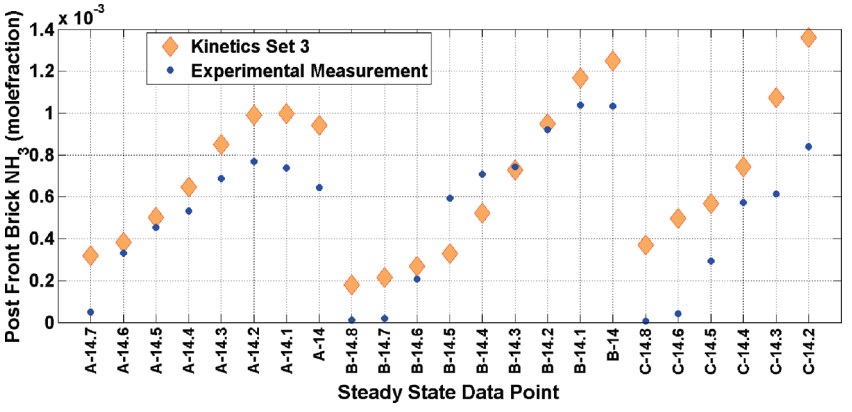

Figure 12. Performance of Kinetics Set 3 for steady-state data. *X*-axis label represent the engine condition (A, B, C) and the air-to-fuel ratio. Engine condition A: 1500 rpm/1.5 bar; B: 2000 rpm/2 bar; C: 2800 rpm/3.5 bar.

NH_3 interaction with ceria cannot be a cause of this delay because there is no Ceria in the front bricks. Additionally, we observe that this lag is higher during the initial portions of the experiment, that is, at lean AFRs (14.6, 14.5) and as the experiment progresses toward rich AFRs (13.9, 13.8), this lag disappears. It has been observed that there is a possibility of the palladium catalyst having some oxygen storage capacity (in lean conditions, Pd stores oxygen by forming PdO)[27−31] and we believe that this oxidized palladium may cause some oxidation of the NH_3 formed under rich conditions. The formation of PdO depends on the operating conditions and as can be formed when the engine is running lean, there are more chances of PdO formation and hence the delay is longer during the lean operation and this delay reduces as we move to rich operation. However, in this work we are interested in global reaction mechanisms for NH_3 oxidation and hence do not model this effect as this would need a

dx.doi.org/10.1021/ie2017866 |*Ind. Eng. Chem. Res.* 2012, 51, 1198–1208

microkinetic approach for Pd-based reactions. Figures 10 and 11 show the performance of this Kinetics Set for controlled transient data pertaining to engine conditions B and C, respectively. The kinetics perform well for engine condition B and reasonably well for engine condition C though the first NH_3 peak is not predicted well for both engine condition B and C. Figure 12 shows the performance of Kinetics Set 3 for steady-state data. Kinetics Set 3 performs reasonably well for steady-state data (and the predictions are much better than that obtained using Kinetics Set 1 and set 2, compare Figures 5 and 12) and is also able to simulate all the data-points successfully. Additionally, Kinetics Set 3 is able to qualitatively capture the observed maximum in NH_3 concentration for engine condition A.

SUMMARY

The focus of this work is on the kinetic modeling of NH_3 formation and oxidation reactions in a three way catalyst (TWC). Controlled steady-state and transient test cell experiments were performed at different air-to-fuel ratios and different engine conditions. This data was used to expand the existing TWC global reaction mechanism[6,8] to account for NH_3 formation and oxidation. The following three additional global reactions were added to the TWC global reaction mechanism.

(a) NH_3 formation

$$NO + 2.5H_2 \rightarrow NH_3 + H_2O$$

(b) NH_3 oxidation with oxygen

$$NH_3 + 1.25O_2 \rightarrow NO + 1.5H_2O$$

(c) NH_3 oxidation with NO

$$NH_3 + 1.5NO \rightarrow 1.25N_2 + 1.5H_2O$$

The experimental data was used to estimate the kinetic parameters of the above reactions (using a one-dimensional mathematical model for the TWC) through optimization techniques. A combination of DIRECT global and COBYLA local optimization algorithm was used for optimization purposes. The objective function formulation (which was limited to reactant species) from Sampara et al.[32] was modified to include product species and to improve the robustness. The estimated kinetic parameters are able to predict the steady-state and controlled transient experimental data reasonably well.

The kinetic model obtained in this work can be used to obtain an improved understanding of the passive ammonia-SCR (TWC-SCR) exhaust architecture for lean burn gasoline engines and can potentially be extended to all lean burn engines (i.e., diesel engines as well). Additionally, this model can be used for control algorithm development purposes to estimate when and for how long the engine should be operated under fuel-rich conditions for producing enough NH_3 (for use in downstream SCR) in the TWC.

Though the estimated kinetic parameters are able to predict the experimental data fairly well, there are a few discrepancies in quantitatively predicting the steady-state data (the qualitative trends are captured correctly) and this could be because of the exclusion of the NH_3 decomposition reaction (to N_2)[15] and additional controlled experiments are needed to validate this. Also, the kinetic parameters obtained in this work needs to be validated over a wider range of temperatures (specifically at lower temperatures). It is expected that N_2O formation (through NH_3 oxidation with NO or O_2)[15] could become significant at lower temperatures and these additional reactions need to be included to simulate lower temperatures. Since it is difficult to perform experiments on a transient engine dynamometer at these low temperatures, a lab-scale reactor setup with controlled feed-gas is being considered and this work is in progress and will be reported in future publication. Despite the limitations of the kinetic model obtained, the kinetic parameters obtained in this work is expected to be a good starting point for further refinement of kinetics when experimental data over a wider range of operating conditions becomes available.

APPENDIX: PARAMETER ESTIMATION SET-UP

In this section, we describe in detail the objective function formulation and the choice of optimization algorithm.

Objective Function Formulation. A log-based objective function formulation for reactant species (i.e., the species present in the inlet feed) was found to be very effective for parameter estimation purposes.[32] However, apart from tracking the reactant species, we are more interested in the amount of NH_3 formed and consumed in the TWC. Hence, the objective function formulation was modified to take into account the least square error for product species (i.e., NH_3). We first discuss the objective function formulation for reactant species and later describe modifications to the formulation for product species.

a. For Reactant Species. The formulation of the objective function by Sampara et al.[32] is based on conversion of the reactant species.

(a) For large conversions (>50%), the absolute magnitude of predicted species concentration at outlet ($x^{p}_{g,i}$) is compared against measured species concentration at outlet ($x^{m}_{g,i}$).

(b) For small conversions ($\leq$50%), the predicted difference between inlet and outlet species concentration ($\Delta x^{p}_{g,i} = x^{in}_{g,i} - x^{p}_{g,i}$) is compared against measured difference between inlet and outlet species concentration ($\Delta x^{m}_{g,i} = x^{in}_{g,i} - x^{m}_{g,i}$).

The criterion to switch between the above two formulations is kept at conversion efficiency of 50%.[32] Hence, for the reactant species, objective function f is defined as below

$$f = \frac{1}{nsp}\sum_{i=1}^{nsp}\left[\log^2\left[\frac{\Delta x^{p}_{g,i}}{\Delta x^{m}_{g,i}}\right]_{conv \leq 50\%} + \log^2\left[\frac{x^{p}_{g,i}}{x^{m}_{g,i}}\right]_{conv > 50\%}\right] \quad (A1)$$

where conversion is defined as

$$conv = \frac{\Delta x^{m}_{g,i}}{x^{in}_{g,i}} \times 100 \quad (A2)$$

and *nsp* represents the various species present in the exhaust feed. However, the above objective function definition can lead to the objective function having infinite values when the numerator of the logarithmic terms are zero and this can lead to difficulty in the optimization process. To overcome this difficulty, eq A1 is modified to ensure that the logarithmic terms do not become zero during optimization:

(a) For small measured conversions (i.e., conv ≤ 50%), the model may predict zero conversion for *i*th species (i.e., $\Delta x^{p}_{g,i} = 0$ as compared to a finite measured conversion (i.e., $\Delta x^{m}_{g,i} > 0$). In such a case, predicted species conversion is set to a small value (10^{-7}). This small value is chosen to be at least 1 order of magnitude lower than the instrument errors in measurement for various species.

(b) For large measured conversions (i.e., conv ≤ 50%), model kinetics may predict zero species concentration ($x^{p}_{g,i} = 0$) at outlet against a finite measured outlet species concentration ($x^{m}_{g,i} > 0$). In such a case, predicted outlet species concentration is set to a small value (10^{-7}).

Accounting for the above two special cases, the objective function definition in eq A1, for reactant species, can be written as

$$f = \frac{1}{nsp}\sum_{i=1}^{nsp}\left[\log^2\left[\frac{\Delta x^{p}_{g,i}}{\Delta x^{m}_{g,i}}\right]_{\text{conv} \le 50\%,\, \Delta x^{p}_{g,i} > 0} + \log^2\left[\frac{10^{-7}}{\Delta x^{m}_{g,i}}\right]_{\text{conv} \le 50\%,\, \Delta x^{p}_{g,i} = 0} + \log^2\left[\frac{x^{p}_{g,i}}{x^{m}_{g,i}}\right]_{\text{conv} > 50\%,\, x^{p}_{g,i} > 0} + \log^2\left[\frac{10^{-7}}{x^{m}_{g,i}}\right]_{\text{conv} > 50\%,\, x^{p}_{g,i} = 0}\right] \quad \text{(A3)}$$

b. For Product Species. In case of NH_3, which is a product species, the measured inlet concentration is always zero as the amount of NH_3 present in engine-out exhaust gas is negligible and is produced in the TWC only. In such a case, conversion cannot be calculated as per the definition in eq A2. Hence *f*, for NH_3, is calculated as below:

$$f_{NH_3} = \log^2\left[\frac{x^{p}_{g,i}}{x^{m}_{g,i}}\right]_{x^{p}_{g,i} > 0} + \log^2\left[\frac{10^{-7}}{x^{m}_{g,i}}\right]_{x^{p}_{g,i} = 0} \quad \text{(A4)}$$

Equations A3 and A4 together provide the complete definition of the objective function:

$$f = \frac{1}{nsp}\sum_{i=1}^{nsp}\left\{\left(\log^2\left[\frac{\Delta x^{p}_{g,i}}{\Delta x^{m}_{g,i}}\right]_{\text{conv} \le 50\%,\, \Delta x^{p}_{g,i} > 0} + \log^2\left[\frac{10^{-7}}{\Delta x^{m}_{g,i}}\right]_{\text{conv} \le 50\%,\, \Delta x^{p}_{g,i} = 0} + \log^2\left[\frac{x^{p}_{g,i}}{x^{m}_{g,i}}\right]_{\text{conv} > 50\%,\, x^{p}_{g,i} > 0} + \log^2\left[\frac{10^{-7}}{x^{m}_{g,i}}\right]_{\text{conv} > 50\%,\, x^{p}_{g,i} = 0}\right)_{nsp \neq NH_3} + \left(\log^2\left[\frac{x^{p}_{g,i}}{x^{m}_{g,i}}\right]_{x^{p}_{g,i} > 0} + \log^2\left[\frac{10^{-7}}{x^{m}_{g,i}}\right]_{x^{p}_{g,i} = 0}\right)_{nsp = NH_3}\right\} \quad \text{(A5)}$$

While summing the errors over various species concentrations to calculate the objective function, a few data points are encountered where some of the measured species concentrations/conversion levels are less than the corresponding experimental error. Such data points are dropped and not included in the calculation of the objective function because such data indicates either zero or 100% conversion thus containing no significant kinetic information.[32] In short, we do not include data points for any species for which $x^{in}_{g,i}$ or $\Delta x^{m}_{g,i}$ is below the following limits:[32]

(i) 5 ppm for NO, CO, and NH_3
(ii) 3 ppm for H_2
(iii) 10 ppm for HC

Hence, only those data points were *admissible* for which at least one species data was above the lower cutoff limits based on experimental error. Out of a total of 27 steady-state data-points, 23 data-points were *admissible* as the rest 4 data-points did not satisfy the cutoff limits based on the above-mentioned experimental error.

Optimization Algorithm. We use an optimization algorithm that is a combination of exploratory and local optimization methods. A batch optimization program,[33,34] which combines DIRECT global optimization algorithm and COBYLA non-smooth local optimization algorithm is used for this work. It uses both local and global search algorithms and is found to be more successful in kinetic parameter estimation.[8]

AUTHOR INFORMATION

Corresponding Author

*E-mail: karthik.ramanathan@gm.com.

Present Addresses

[‖]Laboratory of Thermodynamics in Emerging Technologies (LTNT), Department of Mechanical and Process Engineering (DMAVT), Swiss Federal Institute of Technology (ETH), Zurich.

ACKNOWLEDGMENT

The authors thank Atul Pant, Se Oh, and Kevin L. Perry (all from GM Global R&D Center) for discussions and comments on model performance and engine dynamometer experiments. The authors also would like to thank James D. LaMothe and Albert L. Jewel for their support in running and collecting the engine dynamometer data.

REFERENCES

(1) Pancotti, C.; Pontoppidan, M.; Francia, P.; Montanari, G.; Damasceno, C. F. DGI—Direct gasoline injection status of development for spark-ignited engines. *SAE Tech. Pap. Ser.* **2002** No. 2002-01-3519.

(2) Landenfeld, T.; Kufferath, A.; Gerhardt, J. Gasoline direct injection—SULEV emission concept. *SAE Tech. Pap. Ser.* **2004** No. 2001-01-004.

(3) Li, W.; Perry, K. L.; Narayanaswamy, K.; Kim, C. H.; Najt, P. Passive Ammonia SCR System for Lean-Burn SIDI Engines. *SAE Int. J. Fuels Lubr.* **2010**, *3*, 99–106.

(4) Kim, C. H.; Perry, K.; Viola, M.; Li, W.; Narayanaswamy, K. Three-way catalyst design for urealess passive ammonia SCR: Lean-burn SIDI aftertreatment system. *SAE Tech. Pap. Ser.* **2011** No. 2011-01-0306.

(5) Heeb, N. V.; Forss, A.-M.; Brühlmann, S.; Lüscher, R.; Saxer, C. J.; Hug, P. Three-way catalyst-induced formation of ammonia--velocity- and acceleration-dependent emission factors. *Atmos. Environ.* **2006**, *40* (31), 5986–5997.

(6) Rao, S. K.; Imam, R.; Ramanathan, K.; Pushpavanam, S. Sensitivity analysis and kinetic parameter estimation in a three way catalytic converter. *Ind. Eng. Chem. Res.* **2009**, *48* (8), 3779–3790.

(7) Oh, S. H.; Cavendish, J. C. Transients of monolithic catalytic converters: Response to step changes in feedstream temperature as

related to controlling automobile emissions. *Ind. Eng. Chem. Prod. Res. Dev.* **1982**, *21* (1), 29–37.

(8) Ramanathan, K.; Sharma, C. S. Kinetic parameters estimation for three way catalyst modeling. *Ind. Eng. Chem. Res.* **2011**, *50* (17), 9960–9979.

(9) Lindholm, A.; Currier, N.; Yezerets, A.; Olsson, L. A kinetic study of NOx reduction over Pt/SiO_2 model catalysts with hydrogen as the reducing agent. *Top. Catal.* **2007**, *42*−*43* (1), 83–89.

(10) Clayton, R. D.; Harold, M. P.; Balakotaiah, V. NOx storage and reduction with H_2 on $Pt/BaO/Al_2O_3$ monolith: Spatio-temporal resolution of product distribution. *Appl. Catal., B* **2008**, *84* (3−4), 616–630.

(11) Mulla, S. S.; Chaugule, S. S.; Yezerets, A.; Currier, N. W.; Delgass, W. N.; Ribeiro, F. H. Regeneration mechanism of $Pt/BaO/Al_2O_3$ lean NOx trap catalyst with H_2. *Catal. Today* **2008**, *136* (1−2), 136–145.

(12) Lietti, L.; Nova, I.; Forzatti, P. Role of ammonia in the reduction by hydrogen of NOx stored over $Pt\text{-}Ba/Al_2O_3$ lean NOx trap catalysts *J. Catal.* **2008**, *257* (2), 270–282.

(13) Pérez-Ramírez, J.; Kondratenko, E. V. Mechanism of ammonia oxidation over oxides studied by temporal analysis of products. *J. Catal.* **2007**, *250* (2), 240–246.

(14) Lindholm, A.; Currier, N. W.; Li, J.; Yezerets, A.; Olsson, L. Detailed kinetic modeling of NOx storage and reduction with hydrogen as the reducing agent and in the presence of CO_2 and H_2O over a Pt/Ba/Al catalyst. *J. Catal.* **2008**, *258* (1), 273–288.

(15) Pihl, J. A.; Parks, J. E.; Daw, C. S.; Root, T. W. Product selectivity during regeneration of lean NOx trap catalysts. *SAE Tech. Pap. Ser.* **2006** No. 2006-01-3441.

(16) Kočí, P.; Plát, F.; Štěpánek, J.; Bártová, S.; Marek, M.; Kubíček, M.; Schmeißer, V.; Chatterjee, D.; Weibel, M. Global kinetic model for the regeneration of NOx storage catalyst with CO, H_2, and C_3H_6 in the presence of CO_2 and H_2O. *Catal. Today* **2009**, *147* (Suppl), S257–S264.

(17) Olsson, L.; Sjövall, H.; Blint, R. J. A kinetic model for ammonia selective catalytic reduction over Cu-ZSM-5. *Appl. Catal., B* **2008**, *81* (3−4), 203–217.

(18) Kraehnert, R.; Baerns, M. Kinetics of ammonia oxidation over Pt foil studied in a micro-structured quartz-reactor. *Chem. Eng. J.* **2008**, *137* (2), 361–375.

(19) Scheibe, A.; Hinz, M.; Imbihl, R. Kinetics of ammonia oxidation on stepped platinum surfaces: II. Simulation results. *Surf. Sci.* **2005**, *576* (1−3), 131–144.

(20) Votsmeier, M.; Scheuer, A.; Drochner, A.; Vogel, H.; Gieshoff, J. Simulation of automotive NH_3 oxidation catalysts based on pre-computed rate data from mechanistic surface kinetics. *Catal. Today* **2010**, *151* (3−4), 271–277.

(21) Chatterjee, D.; Kocí, P.; Schmeißer, V.; Marek, M.; Weibel, M.; Krutzsch, B. Modelling of a combined NOx storage and NH_3-SCR catalytic system for Diesel exhaust gas aftertreatment. *Catal. Today* **2010**, *151* (3−4), 395–409.

(22) Kočí, P.; Plát, F.; Štěpánek, J.; Kubíček, M.; Marek, M. Dynamics and selectivity of NOx reduction in NOx storage catalytic monolith. *Catal. Today* **2008**, *137* (2−4), 253–260.

(23) Wei, J.; Becker E, R. The optimum distribution of catalytic material on support layers in automotive catalysis. *Adv. Chem.* **1975**, *143*, 116–132.

(24) Oh, S. H.; Bissett, E. J.; Battiston, P. A. Mathematical modeling of electrically heated monolith converters: Model formulation, numerical methods, and experimental verification. *Ind. Eng. Chem. Res.* **1993**, *32* (8), 1560–1567.

(25) Xu, J.; Harold, M. P.; Balakotaiah, V. Microkinetic modeling of steady-state $NO/H_2/O_2$ on $Pt/BaO/Al_2O_3$ NOx storage and reduction monolith catalysts. *Appl. Catal., B* **2009**, *89* (1−2), 73–86.

(26) Vajo, J. J.; Tsai, W.; Weinberg, W. H. Mechanistic details of the heterogeneous decomposition of ammonia on platinum. *J. Phys. Chem.* **1985**, *89* (15) , 3243−3251.

(27) Gandhi, H. S.; Graham, G. W.; McCabe, R. W. Automotive exhaust catalysis. *J. Catal.* **2003**, 433–442.

(28) Graham, G. W.; Potter, T.; Baird, R. J.; Gandhi, H. S.; Shelef, M. Surface composition of polycrystalline Pd15Rh following high temperature oxidation in air. *J. Vac. Sci. Technol., A* **1986**, *4* (3), 1613–1616.

(29) Lambrou, P. S.; Costa, C. N.; Christou, S. Y.; Efstathiou, A. M. Dynamics of oxygen storage and release on commercial aged Pd-Rh three-way catalysts and their characterization by transient experiments. *Appl. Catal., B* **2004**, *54* (4), 237–250.

(30) Fernandes, D. M.; Alcover Neto, A.; Cardoso, M. J. B.; Zotin, F. M. Z.Commercial automotive catalysts: Chemical, structural and catalytic evaluation, before and after aging. *Catal. Today* **2008**, *133*−*135*, 574–581.

(31) Ivanova, A. S.; Slavinskaya, E. M.; Gulyaev, R. V.; Zaikovskii, V. I.; Stonkus, O. A.; Danilova, I. G.; Plyasova, L. M.; Polukhina, I. A.; Boronin, A. I. Metal-support interactions in Pt/Al_2O_3 and Pd/Al_2O_3 catalysts for CO oxidation. *Appl. Catal., B* **2010**, *97* (1−2), 57–71.

(32) Sampara, C. S.; Bissett, E. J.; Chmielewski, M. Global kinetics for a commercial diesel oxidation catalyst with two exhaust hydrocarbons. *Ind. Eng. Chem. Res.* **2008**, *47* (2), 311–322.

(33) Jones, D. R. The DIRECT Global Optimization Algorithm. In *Encyclopedia of Optimization*; Floudas, C. A.; Pardalos, P. M., Eds.; Kluwer Academic Publishers: Boston, 2001; Vol. 1, pp 431−440.

(34) Jones, D. R.; Perttunen, C. D.; Stuckman, B. E. Lipschitzian optimization without the Lipschitz constant. *J. Optim. Theory Appl.* **1993**, *79* (1), 157–181.

NOTE ADDED AFTER ASAP PUBLICATION

After this paper was published online January 10, 2012, a correction was made to the *Approach (a)* text in the section Parameter Estimation Runs and Results. The corrected version was published January 12, 2012.